Research article

Ryohei Yasukuni, Raymond Gillibert, Mohamed N. Triba, Ruta Grinyte, Valery Pavlov and Marc Lamy de la Chapelle*

Quantitative analysis of SERS spectra of MnSOD over fluctuated aptamer signals using multivariate statistics

https://doi.org/10.1515/nanoph-2019-0041
Received February 11, 2019; revised April 3, 2019; accepted April 3, 2019

Abstract: Surface-enhanced Raman scattering (SERS) sensors using specific aptamers often show difficulties in quantitative analysis because the instable aptamer structures show fluctuated background signals. In this communication, we address the quantitative analysis of the SERS spectra of manganese superoxide dismutase (MnSOD) in different concentrations over the signal arisen from its specific aptamer using multivariate statistical analysis. MnSOD is a primary antioxidant enzyme protecting normal tissue against oxidative stress and is known as a cancer biomarker. By applying principal component analysis, SERS spectra were distinguished when MnSOD was present in a specimen even at 10 pM. The relation between SERS spectra and MnSOD concentrations calculated by partial least-squares regression predicted MnSOD concentrations within one order of magnitude. Moreover, statistically obtained spectral correlations reveal that spectral differences did not originate from additional peaks of MnSOD but from the thermodynamic stability of the aptamer structures. These results open new paths for detection and analytical strategies of SERS-based biosensors using aptamers.

Keywords: SERS; sensor; MnSOD; aptamer; multivariate analysis.

1 Introduction

Improvement of bio-molecular sensing techniques in clinical applications is of utmost importance for a better diagnosis and a monitoring prognosis of diseases in rising populations needing medical care. Easy, fast, inexpensive and reliable bio-sensors for various biological markers have been developed using different types of detection mechanisms such as electrochemistry and optical detections [1–3]. Among these techniques, surface-enhanced Raman scattering (SERS) detections have been gaining attention [4–11]. SERS is the phenomenon in which Raman scattering efficiency increases drastically at the surface of noble metal nanostructures, which arises from a locally enhanced electromagnetic (EM) field through an excitation of localized surface Plasmon resonance (LSPR) of metal nanostructures [12–15]. The SERS vibration spectrum represents physicochemical states of molecules [16] with single molecular sensitivity under optical microscopes [17], permitting acquisitions of the spectral signal from a small volume of dilute target solutions. Moreover, label-free sensing is an important requirement for the development of easy and fast bio-sensing systems [18]. The SERS technique does not require labeling target molecules, and it allows the use of a specimen as taken from the body.

We recently reported a highly sensitive SERS-based manganese superoxide dismutase (MnSOD or also known as SOD2) sensing system in body fluids [19]. MnSOD is one of the primary antioxidant enzymes protecting normal tissue against oxidative stresses, and its activity is linked to the

***Corresponding author: Marc Lamy de la Chapelle,** IMMM – UMR 6283 CNRS, Le Mans Université, Avenue Olivier Messiaen, 72085 Le Mans, Cedex 9, France, e-mail: marc.lamydelachapelle@univ-lemans.fr
Ryohei Yasukuni: Graduate School of Science and Technology, Nara Institute of Science and Technology, Ikoma, Nara, 630-0192, Japan; and Université Paris 13, Sorbonne Paris Cité, Laboratoire CSPBAT, CNRS UMR 7244, Bobigny F-93017, France
Raymond Gillibert: Université Paris 13, Sorbonne Paris Cité, Laboratoire CSPBAT, CNRS UMR 7244, Bobigny F-93017, France; and Horiba Jobin Yvon SAS, Villeneuve-d'Ascq 59650, France
Mohamed N. Triba: Université Paris 13, Sorbonne Paris Cité, Laboratoire CSPBAT, CNRS UMR 7244, Bobigny F-93017, France
Ruta Grinyte and Valery Pavlov: Biofunctional Nanomaterials Department, CIC biomaGUNE, Parque tecnológico de San Sebastian, Donostia-San Sebastian 20009, Spain

development of various carcinomas [20]. Thus, the MnSOD concentration in body fluids is a good bio-marker to provide diagnoses for tumor stages [21]. We have specifically detected SERS signals from MnSOD in serum and saliva using artificial oligonucleotides called aptamers, which are designed to have a strong affinity with the target molecules. Aptamer is becoming an important molecular tool for bio-sensor applications and an alternative to anti-bodies because of its easy synthesis and high chemical stability [22].

In our system, an Au nanocylinder array was fabricated by electron beam lithography (EBL) for exploiting SERS. It showed better SERS signal reproducibility than chemically synthesized colloidal nanoparticle systems. The Au nanocylinder substrate was functionalized by a specific aptamer to MnSOD owing to its thiol head group, and a sample solution containing MnSOD was deposited on the substrate (Figure 1). SERS spectral changes in the presence of MnSOD were successfully detected from the nM range over the SERS spectrum of the aptamer. However, as typical of other SERS sensors using an aptamer, the SERS signal from the aptamer was rather strong compared to target proteins, and it showed complicated signal variations even on the EBL SERS substrate. This is because nucleotides, components of aptamer, normally have bigger Raman cross-sections than proteins, and their long chain does not have one fixed structure [23]. The aptamer size is also a problem because the localized EM field generated by LSPR excitation exponentially decays from the surface of metal nanostructures. Therefore, Raman signals from the aptamer were enhanced stronger than target proteins grafted at a top of the aptamer. Quantitative analysis of the mixed SERS spectra of proteins and aptamers is thus still a challenge for this type of bio-sensors.

In this context, we applied a statistical approach, specifically partial least-squares regression (PLSR), to analyze small SERS spectral changes depending on the concentration of MnSOD in a specimen together with the strong aptamer signal. PLSR is one of the common multivariate techniques for the quantitative analysis of spectral data sets [24, 25]. PLSR creates an assumed model and extracts spectral features related to supervised variables (e.g. concentrations), and is suitable in the system including random factors as signal fluctuations of the aptamer in our case. Although application of PLSR to analyze spectral data sets is not conceptually new, the results demonstrate that protein concentrations are predictable even over a fluctuated aptamer signal. More interestingly, this work finds out that the signal fluctuation of an aptamer itself would be a sensitive indicator of concentrations of target proteins through restriction of the aptamer's structural variations.

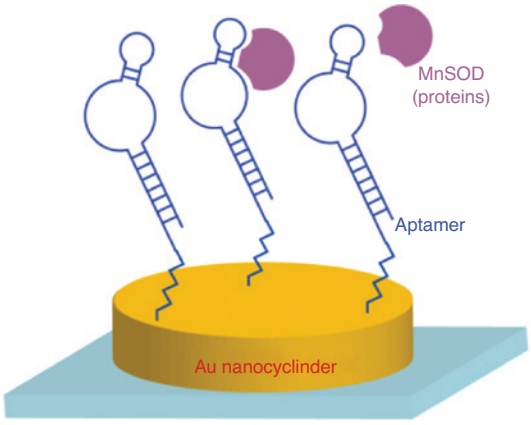

Figure 1: Schematic of the SERS sensor of MnSOD using a specific aptamer.

2 Materials and methods

2.1 Synthesis of the specific aptamer to MnSOD

The aptamer with the following sequence was synthesized with a 3400 DNA synthesizer (Applied Biosystems, Thermo Fisher Scientific Inc., Waltham, MA, USA) and purified with oligonucleotide purification cartridges (Applied Biosystems): 5′-HS-C_6-TT TTT TTT TTT TTT TTC TTC TCT AGC TGA ATA ACC GGA AGT AAC TCA TCG TTT CGA TGA GTT ACT TCC GGT TAT TCA GCT AGA GAA G-3′. The specific sequence to MnSOD was found by the Systematic Evolution of Ligands by EXponential enrichment (SELEX) method. A thiol group was inserted by using 1-O-(4.4′-dimethoxytrityl)-hexyl-disulfide, 1′-[(2-cyanoethyl)-(N,N-diisopropyl)]-phosphoramidite (5′-thiol-modifier C6 S-S CE phosphoramidite). All reagents required for solid phase oligonucleotides synthesis were purchased from Link Technologies (LGC LINK, Bellshill, Scotland, UK). The final concentration of the synthesized aptamer was determined by measuring absorbance at 260 nm with the ND 1000 Spectrophotometer (NanoDrop).

2.2 Fabrication of Au nanocylinders

Au nanocylinders (diameter: 140 nm, height: 50 nm, period: 200 nm) were designed on a glass substrate with a 3-nm chromium adhesion layer by EBL following the conventional lift-off process. The maximum of the LSPR band of fabricated Au nanocylinders is located around 650 nm (Figure S1), and is red-shifted a few tens of nm after functionalization.

2.3 Functionalization of Au nanocylinders

The Au nanocylinder substrate was first cleaned in a UV oxygen plasma cleaner for 30 min and rinsed with ethanol, and dried by nitrogen flow. Then, the substrate was soaked in 1 mM of 6-mercapto-1-hexanol (MHO) (Sigma-Aldrich, Lyon, France) ethanol solution for 1 h and rinsed by ethanol and dried by nitrogen flow. MHO was used as a blocking layer to avoid direct adsorption of proteins onto the Au surface. The MnSOD aptamer was grafted through an exchange between MHO and the aptamer by the deposition of the aptamer aqueous solution with a concentration of 10 ng/μl in 1 M KCL on the MHO covered substrate for 1 h. After the aptamer functionalization, the substrate was kept wet.

2.4 SERS measurements

The MnSOD solution was prepared by mixing lyophilized MnSOD (LF-P0013, SOD2, Human, Abfrontier) in a working buffer [50 mM Tris-acetate, 100 mM NaCl, 5 mM $MgCl_2$ (Sigma-Aldrich) in Milli-Q water and pH = 8.2]. It normally forms tetramers in the presence of manganese ions as in nature, although we have not checked the molecular weight of MnSOD in the buffer solution. The working buffer containing 0, 10 pM, 1 nM and 100 nM concentrations of the monomer MnSOD solution was deposited on the aptamer-functionalized gold nanocylinder substrate. All SERS experiments were performed on the same substrate under liquid conditions by putting a microscope cover slide on the drop of protein solution. The substrate was washed with the working buffer after the experiment with one concentration, and reused for the following experiment with different MnSOD concentrations.

SERS spectra were recorded with a commercial Raman microspectrometer (Horiba Jobin-Yvon, Xplora). The excitation laser ($\lambda = 660$ nm) was focused through a microscope 100× objective (Olympus, NA: 0.9), and Raman scattering was collected through the same objective. The laser power was 0.4 mW at the sample position. For one SERS spectrum, signals were accumulated 5 times for 5 s. A baseline of raw spectra was subtracted and the treated spectrum was normalized using LabSpec 6 (Horiba Scientific, Villeneuve D'ascq, France) for all multivariate statistical analysis.

2.5 Principal component analysis, partial least-squares regression and cross-validation

When principal component analysis (PCA) is applied to the SERS spectrum, the spectrum is regarded as a linear combination of principal components [26]. These principal components are interpreted as new variables optimally describing the spectrum. A set of weights for each principal component in the linear combination characterize a feature of the SERS spectrum. In practice, the first principal component (PC1) is chosen to express the maximum variability of the spectral data, and the second principal component (PC2) is chosen to express the maximum variability of the remaining information, which is not explained by PC1, etc.

It should be noted here that PCA is a purely mathematical technique, and the obtained principal components are less likely to have direct relations with physicochemical events. In order to clarify the relation between SERS spectra and a presence of MnSOD, covariance was calculated at each wave number of SERS spectra.

PLSR is a linear regression method that we used to predict MnSOD concentrations from weights of spectral components [27]. The component is calculated to express the maximum variability of the spectrum and also to have a linear correlation with the concentration of MnSOD. The prediction ability of the PLSR model was estimated using the Monte Carlo cross-validation (MCCV) method [28].

PCA and cross-validated PLSR models were performed with Matlab (MathWorks, Natick, MA) using homemade algorithms based on the algorithm of commercially available SIMCA software (Umetrics, Umea, Sweden).

3 Results and discussion

Averaged SERS spectra from the aptamer on a gold nanocylinder array with three different concentrations of MnSOD are shown in Figure 2. After functionalization of the aptamer, all SERS spectra were measured using the same substrate in a buffer solution containing 0, 10 pM, 1 nM and 100 nM MnSOD. The appearance of these average spectra is quite similar, and it is almost impossible to find clear features linked to concentration changes by eye, especially when individual spectral variations in the same concentration group are taken into account (Figure S2).

It should be noted that, in our previous report, additional peaks appeared over the signal of aptamer when 100 nM MnSOD solution was deposited on the same SERS substrate [19], which is reproducible when the SERS signal was acquired for a long time more than 1 min. However, long-time signal acquisition causes more signal fluctuations and thus is not suitable for quantitative analysis. Hence, a shorter time signal acquisition for 30 s was employed to obtain a stable signal. While the time evolution of SERS

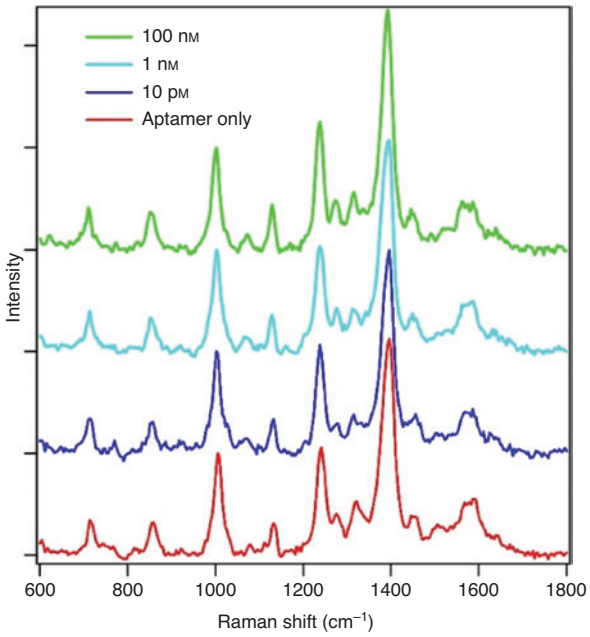

Figure 2: Normalized SERS spectra obtained from (red) only the aptamer, and the aptamer with (blue) 10 pM, (light blue) 1 nM, (green) 100 nM MnSOD.
Each spectrum is an averaged spectrum at 10 different places on the same substrate. A 660 nm CW laser (0.4 mW) was used for SERS excitation and the signal was acquired for 30 s for each spectrum. Background was removed and baseline was offset for clarity.

signals might be related to thermodynamic fluctuations of aptamer and/or MnSOD structures induced by laser heating, its detailed mechanisms are still under discussion.

Precise assignment of aptamer SERS peaks is not easy because four bases have peaks at similar positions, and an aptamer spectrum was not defined as a simple sum of composed nucleotides spectrum but depended on its sequence [29]. Moreover, the conventional Raman spectrum of the aptamer has many more peaks compared to its SERS spectrum (Figure S3). The difference between the conventional Raman and SERS spectra could be explained as follows. Only the part of the aptamer close to the gold surface was detected in SERS, whereas the whole part of the aptamer contributes in the normal Raman spectrum. Indeed, the three main peaks of the aptamer around 1000, 1240 and 1390 cm^{-1} are very similar to that of the 14-thymine part of the aptamer used as a spacer between the thiolated alkane chain and functional polynucleotides to facilitate its immobilization on the Au surface (Figure S4). Given that the thymine spacer has the most contribution in the aptamer signal, three main peaks can be assigned to the rocking, stretching and bending mode of C5-methyl in a thymine base, respectively [30]. The rest of the aptamer sequence probably causes the fluctuation of signals depending on how it interacts with the gold surface.

In order to classify the SERS spectra of aptamer with different concentrations of MnSOD, PCA was first applied for 40 spectra (10 spectra for each group). The weights of PC1 and PC2 in each spectrum are plotted as a score plot in Figure 3A. The spectra acquired in the absence of MnSOD tend to have positive contribution of both PC1 and PC2. In contrast, the spectra acquired in the presence of MnSOD are more likely to have negative contribution of either PC1 or PC2. Hence, the score plot visually discriminates the spectra in the absence of MnSOD from the ones in the presence of MnSOD along the axis from upper right to lower left. The covariance between the presence and absence of MnSOD is shown in Figure 3B. The covariance with high correlation coefficient (in yellow to red) indicates a spectral region strongly related to the presence of MnSOD, which elucidates that the aptamer SERS spectra shifted to a lower frequency when MnSOD was present in a solution. We repeat that the variation of peak

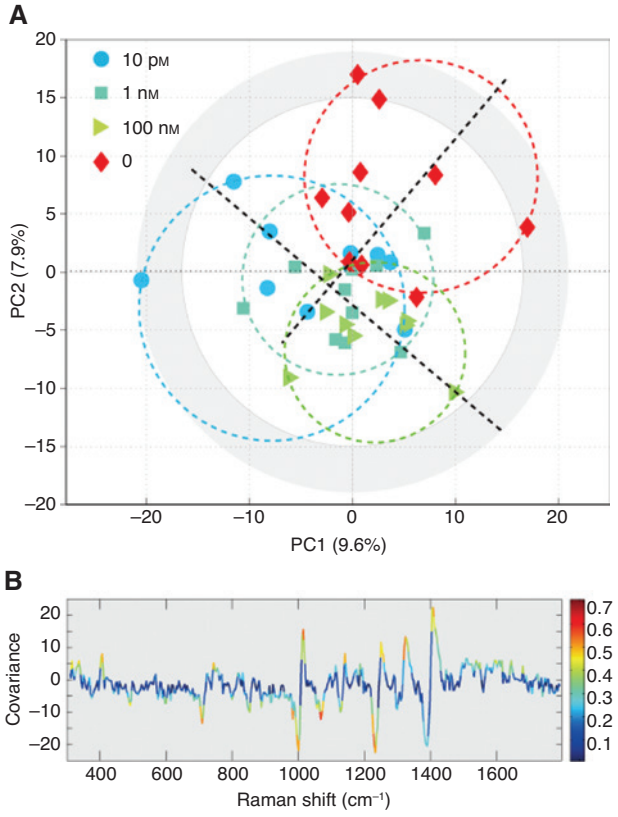

Figure 3: SERS spectral variations by adding MnSOD.
(A) Score plot of PCA for 40 spectra. Concentrations corresponding to each symbol are indicated in the figure. Color dashed circles and dashed lines are guides to see a distribution of symbols and two axes of separation. (B) Covariance between spectral intensities and presence of MnSOD in a solution: 1 or 0 is added in the first row of each SERS spectrum when MnSOD is present or not present in the sample, respectively, and the covariance between the first row and spectral intensities at each wave number is shown in the figure. The color scale indicates correlation coefficient.

frequency was observable depending on sample positions and over time (Figure S2), which could be caused by a structural fluctuation of aptamer. Thus, the frequency shift is thought to be due to the stabilization of aptamer structures by coupling with MnSOD. To be more precise, thermal motion of the thymine spacer would be restricted. A slight decrease of full-width at half-maximum of the main aptamer peaks was observed and supported this hypothesis. Self-stabilization of aptamer in a buffer was also examined, and no spectral shift was confirmed after incubation for 3 h in the buffer without MnSOD.

With regard to the spectral difference depending on MnSOD concentrations, their plots are located square to the axis along the difference between the presence and absence of MnSOD. This orthogonality indicates that the increasing concentration of MnSOD has a different effect on their SERS spectra from the spectral shift. Moreover, the 30 points of three groups with MnSOD are mostly superimposed. The other analytical technique is necessary to discriminate these spectra.

To characterize the spectra from different MnSOD concentrations quantitatively, PLSR was performed for 30 spectra from the concentrations of 10 pM, 1 nM and 100 nM. The PLSR creates a model which relates MnSOD concentrations to an SERS spectral component from their linear correlation. On the basis of the Langmuir-Freundlich surface adsorption model, a number of MnSOD interacted with aptamers at Au nanocylinders surface increased proportional to the logarithm of the MnSOD concentrations in a specimen solution [31]. Thus, we applied the logarithm of the concentrations in the solution as effective concentrations for PLSR.

The PLSR model was created using all SERS spectra in the presence of MnSOD, and by applying the created model to the individual spectrum again, we calculated fitted MnSOD concentrations (Y_{fit}). In Figure 4A, Y_{fit}

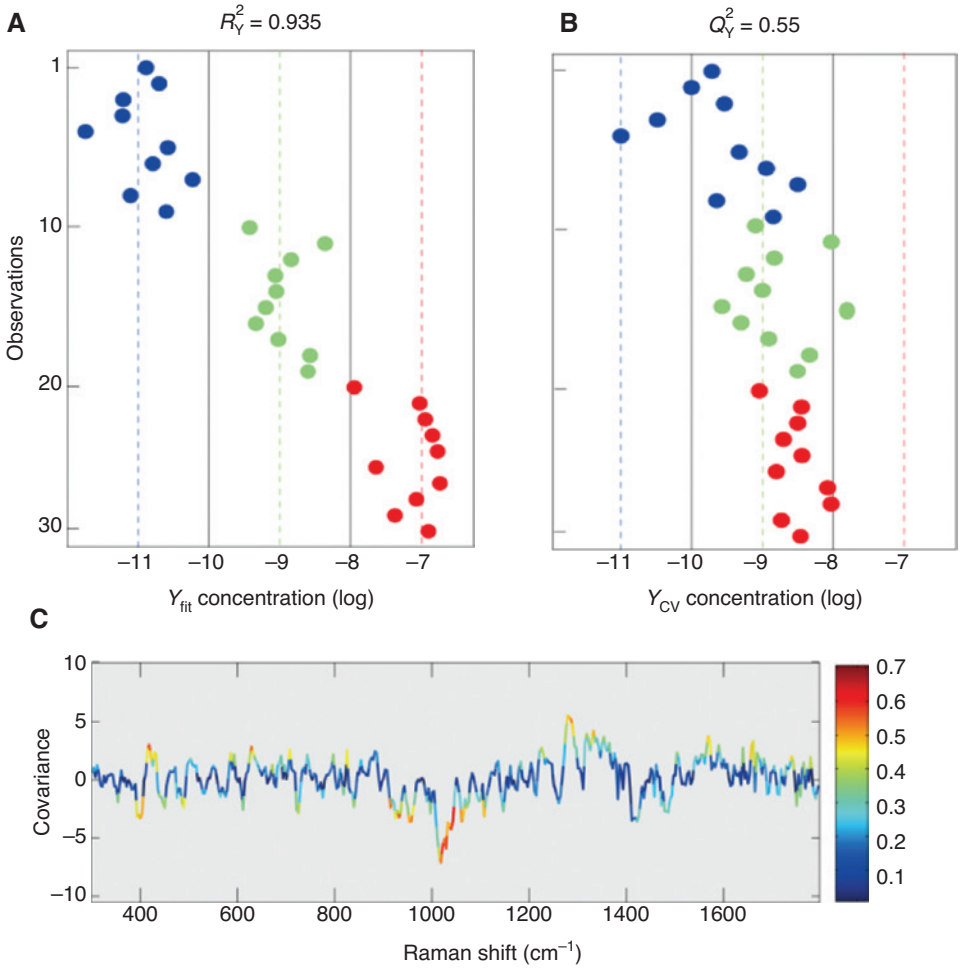

Figure 4: Prediction of MnSOD concentrations from SERS spectral variations.
(A) Concentration fitting and (B) cross-validation prediction of concentrations of SERS spectra acquired from the groups of (blue) 10 pM, (green) 1 nM and (red) 100 nM. (C) Covariance between spectral intensities and MnSOD concentrations: −11 for 10 pM, −9 for 1 nM or −7 for 100 nM was added in the first row of each SERS spectrum depending on added MnSOD concentrations, and the covariance between the first row and spectral intensities at each wave number is shown in the figure. The color scale indicates correlation coefficient.

obtained from each spectrum is represented in line in order of 10 pM, 1 nM and 100 nM from the top. The spectra are fitted into a correct concentration range within one order of magnitude. R_y^2 represents the proportion of the concentration variance explained by the PLSR model. A value of $R_y^2 = 0.935$, which is close to 1, indicates that the 30 spectra are well fitted by the model. In Figure 4C, the covariance between three MnSOD concentrations shows that a small shoulder at slightly higher frequency of the peak at 1000 cm^{-1} has a negative correlation with increasing concentration. This shoulder should become more significant with an increase in MnSOD concentrations if this peak is originated from the SERS peak of MnSOD, namely ring stretching of phenylalanine around 1000 cm^{-1}.

Therefore, we consider that the interaction between MnSOD and aptamer results in this spectral change through the stabilization or alternation of orientation of the spacer thymine part with respect to the gold surface. MCCV was finally carried out to verify the reliability of the created model for unknown samples (Figure 4B) [28]. In this method, we first divided our data, and one part was used to create a model. Then, the created model predicts the other part. This procedure was repeated several times with different patterns of data sets, and the mean value of all the MnSOD concentrations predicted for each spectrum is represented as Y_{cv} in Figure 4B. Q_y^2 is an indicator of the predictability of the model and $Q_y^2 = 1$ means perfect predictability. The plots obtained during the cross-validation procedure were dispersed in an order of magnitude less accurate than the fitting plots, and did not well represent the real concentrations. However, the Q^2 value over 0.5 is indicative of a good ability of the model to predict concentrations [32]. The accuracy of the model can be improved by employing more than three MnSOD concentrations and expanding the number of acquired spectra for each concentration.

4 Conclusions

In conclusion, multivariate statistical analysis was successfully performed to define the characteristics of the SERS spectra of the aptamer and MnSOD in different concentrations. PCA detected the presence of MnSOD even at 10 pM by the spectral shift. Further shift was not observed in the higher MnSOD concentrations, implying that large amounts of aptamers at the Au surface had interacted with MnSOD at 10 pM. Such efficient interaction is unlikely to occur at this low concentration, and therefore there could be a mechanism that accumulates proteins at a laser focal point, for instance, by optical pressure or micro convection by laser heating [33, 34]. Next, PLSR could extract the spectral component depending on MnSOD concentrations and clearly distinguish them. The calculated correlation between SERS spectra and MnSOD concentrations demonstrated that PLSR would be a useful technique for the calibration of protein concentrations from the fluctuated SERS spectra of the protein-aptamer system. This work also pointed out that structural variations of aptamer that resulted from interactions with proteins could be a sensitive indicator to study concentrations of proteins in a specimen. This viewpoint would enable us to overcome an intrinsic problem of the small protein signal using aptamer in the SERS-based detection system.

At the present stage, we have not understood well how the coupling with MnSOD and the increase of its concentration modifies aptamer structures and flexibility. More insights for such interactions enable us to create a more accurate model to calculate MnSOD concentrations in a specimen. We are going to address MnSOD-aptamer interactions by means of a time-resolved single-protein-level SERS experiment, which reveals individual protein/aptamer behavior hidden by signal averaging in time and among multiple proteins/aptamers.

Acknowledgments: This work is supported by the grant PIRANEX project (ANR-12-NANO-0016), the Louise project (ANR-15-CE04-0001) and the Nanobiosensor project (ANR-15-CE29-0026) from the French National Research Agency (ANR). RG and VP acknowledge the Spanish Ministry of Economy and Competitiveness (Projects BIO2014-59741-R) and the Spanish Ministry of Science, Innovation and Universities (Project BIO2017-88030-R).

References

[1] Grieshaber D, MacKenzie R, Voeroes J, Reimhult E. Electrochemical biosensors – sensor principles and architectures. Sensors 2008;8:1400–58.
[2] Willner I, Zayats M. Electronic aptamer-based sensors. Angew Chem Int Ed 2007;46:6408–18.
[3] Howes PD, Chandrawati R, Stevens MM. Colloidal nanoparticles as advanced biological sensors. Science 2014;346:53.
[4] Bantz KC, Meyer AF, Wittenberg NJ, et al. Recent progress in SERS biosensing. Phys Chem Chem Phys 2011;13:11551.
[5] Lane LA, Qian X, Nie S. SERS nanoparticles in medicine: from label-free detection to spectroscopic tagging. Chem Rev 2015;15:10489–529.
[6] McFarland AD, Van Duyne RP. Single silver nanoparticles as real-time optical sensors with zeptomole sensitivity. Nano Lett 2003;3:1057–62.
[7] Grubisha DS, Lipert RJ, Park HY, Driskell J, Porter MD. Femtomolar detection of prostate-specific antigen: an immunoassay based on surface-enhanced Raman scattering and immunogold labels. Anal Chem 2003;75:5936–43.

[8] Strickland AD, Batt CA. Detection of carbendazim by surface-enhanced Raman scattering using cyclodextrin inclusion complexes on gold nanorods. Anal Chem 2009;81:2895–903.
[9] Guillot N, Lamy de la Chapelle M. Lithographied nanostructures as nanosensors. J Nanophotonics 2012;6:64506.
[10] Gillibert R, Lamy de la Chapelle M. Explosive detection by surface enhanced Raman scattering. Trends Anal Chem 2018;105:166–72.
[11] Gillibert R, Triba M, Lamy de la Chapelle M. Surface enhanced Raman scattering sensor for highly sensitive and selective detection of ochratoxin A. Analyst 2018;143:339–45.
[12] Hossain MK, Kitahama Y, Huang GG, Han X, Ozaki Y. Surface-enhanced Raman scattering: realization of localized surface plasmon resonance using unique substrates and methods. Anal Bioanal Chem 2009;394:1747–60.
[13] Jain PK, El-Sayed MA. Plasmonic coupling in noble metal nanostructures. Chem Phys Lett 2010;487:153–60.
[14] Felidj N, Grand J, Laurent G, et al. Multipolar surface plasmon peaks on gold nanotriangles. J Chem Phys 2008;128:094702.
[15] Guillot N, Lamy de la Chapelle M. The electromagnetic effect in surface enhanced Raman scattering: enhancement optimization using precisely controlled nanostructures. J Quant Spectrosc Radiat Transf 2012;113:2321–33.
[16] Cottat M, Yasukuni R, Homma Y, et al. Phosphorylation impact on Spleen Tyrosine kinase conformation by Surface Enhanced Raman Spectroscopy. Sci Rep 2017;7:39766.
[17] LeRu EC, Etchegoin PG. Single-molecule surface-enhanced Raman spectroscopy. Annu Rev Phys Chem 2012;63:65–87.
[18] Irrera A, Leonardi AA, Franco CD, et al. New generation of ultrasensitive label-free optical Si nanowire-based biosensors. ACS Photon 2018;5:471–9.
[19] Cottat M, D'Andrea C, Yasukuni R, et al. High sensitivity, high selectivity SERS detection of MnSOD using optical nanoantennas functionalized with aptamers. J Phys Chem C 2015;119:15532–40.
[20] Oberley LM. Mechanism of the tumor suppressive effect of MnSOD overexpression. Biomed Pharmacother 2005;59:143–8.
[21] Schadendorf D, Zuberbier T, Diehl S, Schadendorf C, Czarnetzki BM. Serum manganese superoxide dismutase is a new tumour marker for malignant melanoma. Melanoma Res 1995;5:351–3.
[22] Ruigrok VJB, Levisson M, Eppink MHM, Smidt H, van der Oost J. Alternative affinity tools: more attractive than antibodies? Biochem J 2011;436:1–13.
[23] Pagba CV, Lane SM, Wachsmann-Hogiu S. Raman and surface-enhanced Raman spectroscopic studies of the 15-mer DNA thrombin–binding aptamer. J Raman Spectrosc 2010;41:241–7.
[24] Lindberg W, Persson J-A, Wold S. Partial least-squares method for spectrofluorimetric analysis of mixtures of humic acid and lignin sulfonate. Anal Chem 1983;55:643–8.
[25] Mendes LS, Oliveira FCC, Suarez PAZ, Rubim JC. Determination of ethanol in fuel ethanol and beverages by Fourier transform (FT)-near infrared and FT-Raman spectrometries. Analytica Chimica Acta 2003;493:219–31.
[26] Bro R, Smilde AK. Principal component analysis. Anal Methods 2014;6:2812–31.
[27] Wold S, Sjöström M, Eriksson L. PLS-regression: a basic tool of chemometrics. Chemom Intell Lab Syst 2001;58:109–30.
[28] Papadopoulou E, Bell STJ. Label-free detection of single-base mismatches in DNA by surface-enhanced Raman spectroscopy. Angew Chem Int Ed 2011;50:9058–61.
[29] Xu Q-S, Liang Y-Z, Du Y-P. Monte Carlo cross-validation for selecting a model and estimating the prediction error in multivariate calibration. J Chemom 2004;18:112–20.
[30] Otto C, van den Tweek TJJ, de Mul FFM, Greve J. Surface-enhanced Raman spectroscopy of DNA bases. J Raman Spectrosc 1986;17:289–98.
[31] Li X, Husson SM. Adsorption of dansylated amino acids on molecularly imprinted surfaces: a surface plasmon resonance study. Biosens Bioelectron 2006;22:336–48.
[32] Wheelock ÅM, Wheelock CE. Trials and tribulations of omics data analysis: assessing quality of SIMCA-based multivariate models using examples from pulmonary medicine. Mol Biosyst 2013;9:2589.
[33] Enders M, Mukai S, Uwada T, Hashimoto S. Plasmonic nanofabrication through optical heating. J Phys Chem C 2016;120:6723–32.
[34] Urban AS, Carretero-Palacios S, Lutich AA, Lohmüller T, Feldmann J, Jäckel F. Optical trapping and manipulation of plasmonic nanoparticles: fundamentals, applications, and perspectives. Nanoscale 2014;6:4458.

Supplementary Material: The online version of this article offers supplementary material (https://doi.org/10.1515/nanoph-2019-0041).